AGU PUBLICATIONS

JGR

Journal of Geophysical Research: Solid Earth

RESEARCH ARTICLE
10.1002/2014JB011755

Key Points:
- In the West Antarctica, there is apparent mass loss acceleration
- The acceleration is caused by precipitation decrease and ice discharge increase
- Mass gain acceleration due to atmospheric pressure is observed in GRACE gravity

Supporting Information:
- Readme

Correspondence to:
K.-W. Seo,
seokiweon@snu.ac.kr

Citation:
Seo, K.-W., C. R. Wilson, T. Scambos, B.-M. Kim, D. E. Waliser, B. Tian, B.-H. Kim, and J. Eom (2015), Surface mass balance contributions to acceleration of Antarctic ice mass loss during 2003–2013, *J. Geophys. Res. Solid Earth*, *120*, 3617–3627, doi:10.1002/2014JB011755.

Received 9 NOV 2014
Accepted 10 APR 2015
Accepted article online 14 APR 2015
Published online 12 MAY 2015

Surface mass balance contributions to acceleration of Antarctic ice mass loss during 2003–2013

Ki-Weon Seo[1], Clark R. Wilson[2,3], Ted Scambos[4], Baek-Min Kim[5], Duane E. Waliser[6], Baijun Tian[6], Byeong-Hoon Kim[1], and Jooyoung Eom[1]

[1]Department of Earth Science Education, Seoul National University, Seoul, South Korea, [2]Department of Geological Sciences, Jackson School of Geosciences, University of Texas at Austin, Austin, Texas, USA, [3]Center for Space Research, University of Texas at Austin, Austin, Texas, USA, [4]National Snow and Ice Data Center, University of Colorado Boulder, Boulder, Colorado, USA, [5]Division of Polar Earth System Sciences, Korea Polar Research Institute, Incheon, South Korea, [6]Jet Propulsion Laboratory, California Institute of Technology, Pasadena, California, USA

Abstract Recent observations from satellite gravimetry (the Gravity Recovery and Climate Experiment (GRACE) mission) suggest an acceleration of ice mass loss from the Antarctic Ice Sheet (AIS). The contribution of surface mass balance changes (due to variable precipitation) is compared with GRACE-derived mass loss acceleration by assessing the estimated contribution of snow mass from meteorological reanalysis data. We find that over much of the continent, the acceleration can be explained by precipitation anomalies. However, on the Antarctic Peninsula and other parts of West Antarctica, mass changes are not explained by precipitation and are likely associated with ice discharge rate increases. The total apparent GRACE acceleration over all of the AIS between 2003 and 2013 is -13.6 ± 7.2 Gt/yr^2. Of this total, we find that the surface mass balance component is -8.2 ± 2.0 Gt/yr^2. However, the GRACE estimate appears to contain errors arising from the atmospheric pressure fields used to remove air mass effects. The estimated acceleration error from this effect is about 9.8 ± 5.8 Gt/yr^2. Correcting for this yields an ice discharge acceleration of -15.1 ± 6.5 Gt/yr^2.

1. Introduction

During the last two decades, the rate of ice mass loss from the Antarctic Ice Sheet (AIS) has averaged about 71 Gt/yr [*Shepherd et al*., 2012], and recent observations suggest acceleration of mass loss of 14.5 Gt/yr^2 [*Rignot et al*., 2011]. Acceleration of this magnitude through 2100 would lead to about 15 cm global mean sea level rise [*Rignot et al*., 2011]. However, there is much uncertainty in this prediction given the short duration of observations [*Wouters et al*., 2013] and continuing study of physical mechanisms [*Bamber and Aspinall*, 2013]. Discerning the relative contributions of increasing ice discharge rates and multiyear precipitation anomalies to this apparent acceleration is an important aspect of any estimate of effects on future sea level. If precipitation anomalies are the main cause of the acceleration, then the current trend might decrease or even reverse in sign in the future.

The importance of surface mass balance (SMB) anomalies for the Greenland Ice Sheet has been demonstrated [*Sasgen et al*., 2012]. *Fettweis et al*. [2013] found that since 2003, an apparent mass loss acceleration is related to a negative surface mass balance (SMB) anomaly linked to the North Atlantic Oscillation (NAO). Given the decadal scale of the NAO, an SMB increase may occur in the future. Likewise, ice loss acceleration over the AIS [*Velicogna*, 2009] may originate from SMB anomalies, as indicated by several recent studies. *Lee et al*. [2012] found that accelerated losses in the Amundsen Sea catchment were partly associated with a precipitation decrease. In East Antarctica, an extreme precipitation anomaly starting in 2009 significantly impacted the overall regional and continental ice mass balance [*Boening et al*., 2012; *Lenaerts et al*., 2012; *Shepherd et al*., 2012]. Finally, from *Sasgen et al*. [2010], we know that interannual ice mass variations in the Antarctic Peninsula and Amundsen Sea catchment are linked to El Niño–Southern Oscillation, and they suggested that precipitation anomalies were the likely cause.

Because anomalous precipitation patterns may obscure understanding of AIS ice discharge acceleration, it is important to separately estimate this SMB effect. Most recently, *Velicogna et al*. [2014] examined AIS mass acceleration using Gravity Recovery and Climate Experiment (GRACE) and compared it with SMB over the continent and five regions including the Antarctic Peninsula, Amundsen Sea sector, Queen Maud Land,

Totten/Moscow/Frost sector, and Victoria/Wilkes land. They showed that SMB changes accounted for ice mass acceleration in some regions, but causes of large acceleration discrepancies between GRACE and SMB in East Antarctic regions were left unresolved. In this study, we expand on this previous work by examining the entire drainage systems within the AIS using GRACE and SMB precipitation estimates from meteorological reanalyses. We show a connection between AIS acceleration and probable atmospheric pressure errors in GRACE estimates, which may account for much of the acceleration discrepancy between GRACE and SMB estimates. Finally, we discuss contributions of ice discharge to ice mass loss acceleration.

2. Data and Methods

Antarctic ice mass balance is a combination of SMB and ice discharge (D):

$$\Delta M_{T_0}^{T} = \int_{T_0}^{T} \mathrm{SMB}\, dt - \int_{T_0}^{T} D\, dt \tag{1}$$

where $\Delta M_{T_0}^{T}$ is the mass change from T_0 to T. SMB is separated into precipitation (P), sublimation (SU), drifting snow erosion (ER), and meltwater runoff (RU) [*van Wessem et al*., 2014]:

$$\mathrm{SMB} = P - \mathrm{SU} - \mathrm{ER} - \mathrm{RU} \tag{2}$$

We ignore sublimation, drifting snow erosion, and meltwater runoff because their contributions to SMB variations in Antarctica are minor [*van Wessem et al*., 2014]. Therefore, Antarctic ice mass balance is simply estimated as the difference between integrated precipitation (P) and ice discharge (D):

$$\Delta M_{T_0}^{T} \approx \int_{T_0}^{T} P dt - \int_{T_0}^{T} D dt \tag{3}$$

Three reanalysis products are used to assess Antarctic precipitation: European Centre for Medium-Range Weather Forecasts (ECMWF) Re-Analysis (ERA) Interim [*Simmons et al*., 2007], National Centers for Environmental Prediction/Department of Energy (NCEP/DOE) [*Kanamitsu et al*., 2002], and Modern-Era Retrospective Analysis for Research and Applications (MERRA) [*Rienecker et al*., 2011]. Because spatial scales of the three products differ, they are resampled to a 1° grid spacing, and a mean value is estimated at each grid point. Antarctic precipitation from regional climate models such as Regional Atmospheric Climate Model version 2.3 (RACMO2.3) [*van Wessem et al*., 2014] would be an alternative choice, but precipitation from reanalyses shows temporal variability in better agreement with ice-penetrating radar and ice core observations [*Medley et al*., 2013]. However, RACMO2.3 results are used as supporting information in estimates of SU, ER, and RU.

Because in situ observations are sparse in Antarctica, it is difficult to directly assess precipitation uncertainty [*Palerme et al*., 2014]. An uncertainty estimate is taken to be the root-mean-square (RMS) difference between the three reanalysis products and their mean. This error estimate is about 29% of the mean field RMS variation.

To estimate $\Delta M_{T_0}^{T}$ for the AIS, we use Center for Space Research Release 05 GRACE monthly gravity solutions. These consist of spherical harmonic (SH) coefficients to degree and order 60, from January 2003 to December 2013. We replace degree 2 order 0 coefficients with satellite laser ranging estimates [*Cheng and Tapley*, 2004] and include degree 1 coefficients estimated from GRACE data and numerical models [*Swenson et al*., 2008]. North-south stripe noise in the gravity solutions is removed from SH order 12 and higher [*Swenson and Wahr*, 2006], and glacial isostatic adjustment (GIA) effects are removed using the ICE-5G GIA model [*A et al*., 2013]. Random noise at high SH degrees is suppressed by Gaussian smoothing. Various smoothing radii are used as described below.

GRACE mass fields with a limited range of SH degrees and additional Gaussian smoothing suffer from spatial leakage error [*Velicogna and Wahr*, 2013]. This is particularly problematic in coastal regions, where leakage into the oceans affects the mass budget for nearby land. We correct leakage error in two different ways: by forward modeling for individual basins and by a scale factor. The forward modeling method [*Chen et al*., 2013] fits gridded GRACE data with 600 km Gaussian smoothing with a mass change field that is entirely on land. There are initial predefined mean ice mass change fields within each basin (Figure 1)

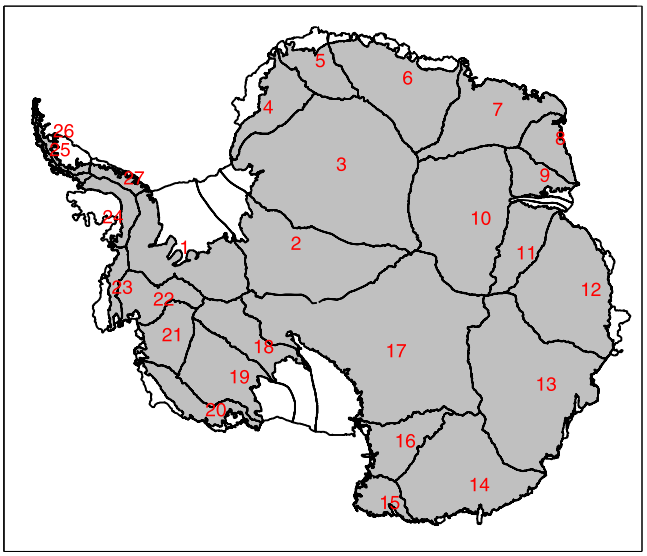

Figure 1. Antarctic basins.

[*Zwally et al.*, 2012] adjusted at each iteration to fit the GRACE data. The eventual goal is to estimate mass change in smaller basins, but initially, a large 600 km Gaussian smoothing radius is necessary to suppress spatial random noise. The initial ice mass fields are filtered with 600 km Gaussian smoothing, and mean values in basins are calculated from the smoothed fields. Mean basin differences between smoothed initial fields and GRACE data are computed and added to update the ice mass field. Iterations continue as the updated field is smoothed by 600 km Gaussian filtering again. An updated field is recomputed until the smoothed updated field is close to the GRACE data within a defined threshold.

The forward modeling approach is useful to examine average ice mass changes within basins but makes limited contributions to understanding spatial variations. As an alternative, a scaling factor approach is used, in which leakage of variance is estimated for each grid element. To estimate scale factors, we define an exact Antarctic continental function, which is 1 inside and 0 outside the continent. The exact function is converted to SH coefficients to degree and order 60, smoothed by a 300 km Gaussian filter, and sampled on a regular latitude-longitude grid. The ratio of the exact basin function to the smoothed basin function at each grid point is the scale factor. GRACE mass fields (300 km Gaussian smoothing) are then adjusted using the scale factor. Precipitation fields are given with high spatial resolution. When represented as a SH expansion to degree 60, leakage error in precipitation fields is corrected using the scale factors. The leakage error would be about 28.5% without applying the scale factors. We estimate associated precipitation error at about 4.8% after the scale factor correction. The scale factor method is an approximate way to address the limited resolution of GRACE, providing a reasonable way to compare spatial patterns of GRACE fields with those of precipitation.

3. Antarctic Ice Mass Balance

3.1. Ice Mass Change in Basins

For the 27 AIS basins [*Zwally et al.*, 2012] (Figure 1), we estimate mass variations from GRACE corrected for leakage by the forward modeling method. The sum of the changes from all basins, Figure 2a, is an

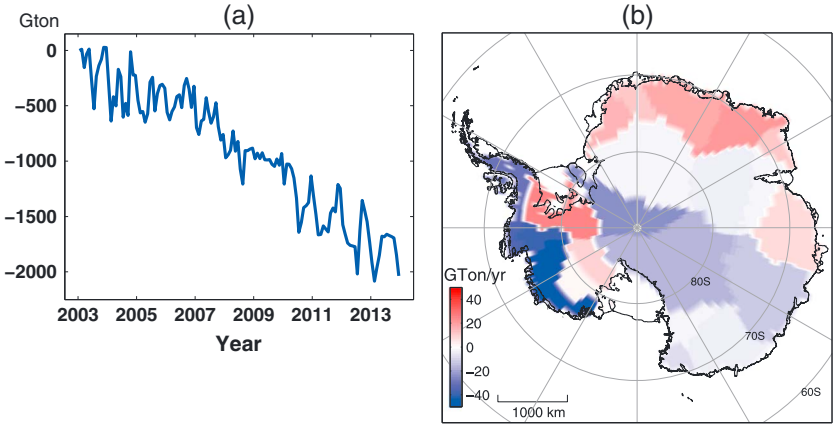

Figure 2. (a) Antarctic ice mass variations and (b) linear trends within each basin from the forward modeling approach.

Antarctic total mass variation time series from January 2003 to December 2013. It shows a strong negative trend. Some seasonal scale variations are evident, though not in all years. The least squares slope and formal uncertainty from Figure 2a is -162.8 ± 30.0 Gt/yr. This is close to a previous mascon estimate [*Schrama et al*., 2014] of -171 ± 22 Gt/yr, which used the same ICE-5G GIA model (February 2003 to September 2013). Our stated uncertainty is a 95% confidence interval considering GRACE noise and misfit of the linear trend to the time series. GRACE noise is estimated from the difference between original and smoothed SH coefficients [*Velicogna and Wahr*, 2013]. The map of linear trends in Figure 2b shows distinct spatial patterns with strong negative trends in West Antarctica (WA) and the Antarctic Peninsula (AP) and weak positive trends in East Antarctica (EA) and interior regions of WA. The negative trends in WA and AP are likely due to ice discharge [*Pritchard et al*., 2009; *Shepherd et al*., 2012], while the positive trends in Dronning Maud Land (DML) are associated with anomalous precipitation accumulation [*Boening et al*., 2012]. The positive trend in the WA interior is associated in part with shutdown of the Kamb Ice Stream flow [*Pritchard et al*., 2012].

The linear trend for Figure 2a or for individual basins (Figure 2b) is strongly dependent on GIA model corrections [*King et al*., 2012]. Further discussion of related uncertainty in the trend is beyond the scope of this study, and we simply subtract the trends from gridded $\Delta M^T_{T_0}$ to remove both constant rate ice mass changes from 2003 to 2013 and any residual GIA effect. We show below that by removing linear trends, the acceleration estimate is insensitive to uncertainties in the GIA model. Additionally, seasonal cycles are subtracted from $\Delta M^T_{T_0}$, and the "residual" fields from 2003 to 2013 are denoted by ΔM^*. In a similar way, we remove linear trends and seasonal cycles at each grid point for precipitation accumulation ($\int_{T_0}^{T} P\,dt$), with the result denoted by P^*.

Figure S1 in the supporting information shows times series of ΔM^* (blue) and P^* (red) from 27 basins. In general, both variations agree well with each other. However, there are some notable differences, for example, in Basins 18, 20, 21 and 23. Differences between ΔM^* and P^* at interannual, and longer time scales would be associated with ice discharge variations and/or interbasin spatial leakage errors in ΔM^*. The forward modeling method is effective in correcting for spatial leakage into the oceans, but ice mass variations in individual basins may still be contaminated by leakage from nearby basins. The limited spatial resolution of GRACE makes it difficult to correct for basin to basin leakage because it is determined not only by basin size and shape but by relative amplitudes and temporal correlation of variations within nearby basins.

Monte Carlo (MC) experiments are used to understand basin to basin leakage error related to basin size and shape. For each basin, an independent synthetic time series of 132 zero mean Gaussian random numbers is generated. These synthetic series all have the same variance and the same length as the monthly January 2003 to December 2013 GRACE time series. The synthetic data for all basins are processed to resemble GRACE data by expanding them into spherical harmonics and smoothing with a 600 km Gaussian filter. Then forward modeling is used to estimate from this GRACE-like data time series of variations within each basin. Correlation coefficients among basin time series are then computed. An ensemble of 100 synthetic data sets is used to compute a mean correlation coefficient (Figure S2a in the supporting information) and associated 95% confidence interval (Figure S2b in the supporting information). The true correlation among basin time series should be zero because the original synthetic time series for each basin are independent. Estimated correlation coefficients significantly larger than zero must be associated with basin to basin leakage. Significantly nonzero correlation coefficients are observed among a number of basins, especially in the AP and WA.

The MC experiments show that it is difficult to interpret ΔM^* in some basins due to leakage error. Consequently, we combine a number of basins to make nine larger regions, denoted as B1 to B9 (with associated basins): B1 (1, 2, and 3), B2 (4, 5, and 6), B3 (7, 8, 9, 10, 11, and 12), B4 (13), B5 (14, 15, and 16), B6 (17), B7 (18, 19, and 20), B8 (21, 22, and 23), and B9 (24, 25, 26, and 27). Figure S3 in the supporting information shows that MC correlation coefficients for these nine regions are effectively zero, since all are smaller than the 95% confidence level. Thus, interbasin leakage error should be negligible, and these larger regions are used to study ΔM^* and P^*.

Another possible error in ΔM^* may be associated with GIA model uncertainty. Linear trends in ΔM^* are removed after forward modeling, so GIA variations (also linear in time) would not be expected to strongly

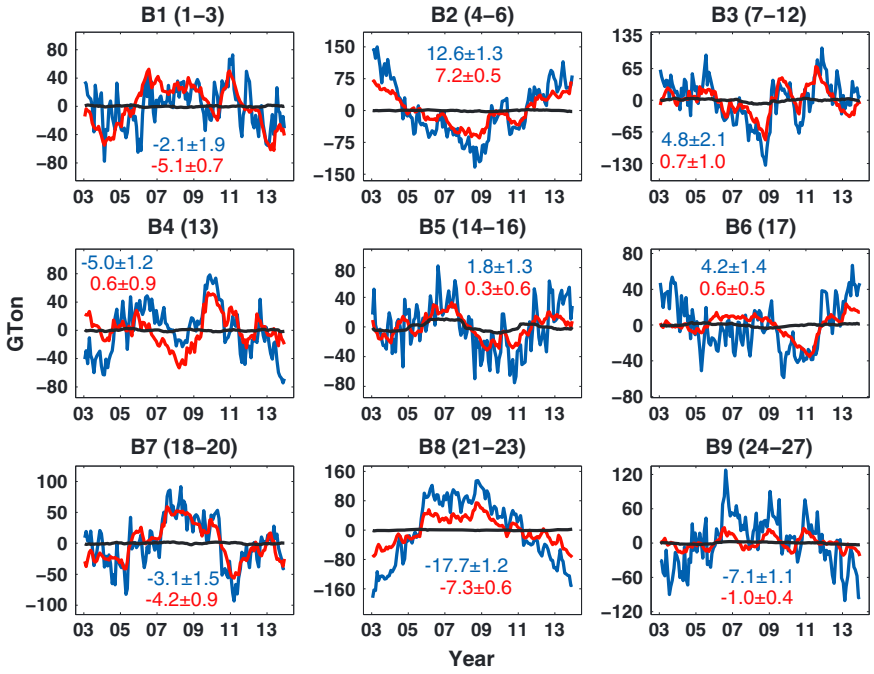

Figure 3. Ice mass variation (ΔM^*) and precipitation accumulation (P^*) in nine regions, B1–B9, after removing linear trends and seasonal cycles from $\Delta M^T_{T_0}$ and $\int_{T_0}^{T} P dt$. The black lines show estimates of combined accumulation from sublimation, drifting snow erosion, and meltwater runoff.

contaminate ΔM^*. However, it is possible that iterative forward modeling may alter linear temporal variations in individual basins. To understand this, we used forward modeling for two additional processing scenarios: one in which no GIA corrections were made and the other in which linear trends in $\Delta M^T_{T_0}$ were removed during forward modeling iterations. The three estimates of ΔM^* are nearly identical, showing that by removing linear trends from all time series, GIA model uncertainty has a negligible effect on our results.

Figure 3 shows time series of GRACE anomalous ice mass variations (ΔM^*, blue) and accumulation anomalies (P^*, red) for the nine regions, B1–B9. The black lines are the RACMO2.3 estimates of other SMB components (SU + ER + RU) showing that they are negligible. The blue and red numbers in Figure 3 are the acceleration rates (Gt/yr^2), corresponding to coefficient a_1 in a least squares fit of the form $a_0 + a_1 \frac{1}{2}(t - t_0)^2$ to ΔM^* and P^*, respectively, where t_0 is the middle of the period from January 2003 to December 2013. In most regions, the two data sets show similar variations, confirming the important role of accumulation in determining acceleration. In particular, Basins 4–6 in the Dronning Maud Land (DML) show clear acceleration of mass gain related to precipitation accumulation [*Boening et al.*, 2012; *Lenaerts et al.*, 2012], while ΔM^* shows a larger rate than P^*. In addition, Basins 1–3 (Region B1) and Basins 7–12 (Region B3) show that distinct interannual variations of ΔM^* are mostly explained by P^*, although ΔM^* and P^* accelerations differ. Basin 13 shows accelerated loss and large interannual variations, which may be interpreted as an ice discharge increase for Totten Glacier. The acceleration in Basin 13 (Region B4) has been estimated in other studies [*Williams et al.*, 2014]. Similar interannual variations of ΔM^* and P^* are exhibited in Basins 14–16 (Region B5) and Basin 17 (B6). Similar to B2 and B3, accelerations rates in B5 and B6 for ΔM^* are larger than for P^*. More similar variations of ΔM^* and P^* appear in Basins 18–20 (B7). For Basins 21–23 (B8), including the Amundsen Sea (AS) sector of WA and AP (24–27) (Region B9), acceleration in ΔM^* exceeds that in P^*, consistent with accelerated ice discharge in those regions [*Rignot et al.*, 2008].

We now calculate the combined regional acceleration rates based on the sum of all basin series (Figure S1 in the supporting information) for the AP, WA, and EA (Table 1). Total AIS mass acceleration for ΔM^* is -13.6 ± 7.2 Gt/yr^2, close to the previous estimate [*Schrama et al.*, 2014] of -12 ± 7 Gt/yr^2. Acceleration of precipitation accumulation P^* is -8.2 ± 2.0 Gt/yr^2 and therefore accounts for a sizable fraction of the overall

Table 1. Ice Mass Loss Acceleration (ΔM^*) for the Antarctic Continent, Antarctic Peninsula, West Antarctica (Amundsen Sea Sector and Non-Amundsen Sea Sector), and East Antarctica (Black Fonts) and Their Contributions From Precipitation Accumulation (P^*)[a]

Drainage Basin	P^*	ΔM^*	ΔM^*	D^*
Antarctica	-8.2 ± 2.0	-13.6 ± 7.2	*-23.3 ± 6.3*	*15.1 ± 6.5*
Antarctic Peninsula	-1.0 ± 0.4	-5.9 ± 1.1	*-6.1 ± 1.0*	*5.0 ± 1.1*
West Antarctica	-14.4 ± 1.4	-24.0 ± 2.2	*-25.7 ± 2.3*	*11.3 ± 2.7*
Amundsen Sea sector (Basins 21 and 22)	-5.0 ± 0.5	-13.6 ± 1.1	*-14.1 ± 1.2*	*9.1 ± 1.3*
Non-Amundsen Sea sector of WA	-9.4 ± 0.8	-10.4 ± 1.8	*-11.6 ± 1.7*	*2.2 ± 1.9*
East Antarctica	7.2 ± 1.8	16.3 ± 5.7	*8.4 ± 5.0*	*-1.2 ± 5.5*

[a]Ice mass loss acceleration (ΔM^*) for those regions after atmospheric pressure error corrections and ice discharge acceleration ($D^* = P^* - \Delta M^*$) are shown in italics. Unit is Gt/yr^2.

acceleration. This result confirms the observation that "ice sheet weather" variations hinder accurate projection of long-term sea level change caused by "ice dynamics" [*Wouters et al*., 2013]. However, differences for the AP, WA, and EA clearly show regional variations in discharge acceleration [*Velicogna et al*., 2014]. AP discharge acceleration is significant since $\Delta M^* = -5.9 \pm 1.1$ Gt/yr^2, while for P^*, the value is -1.0 ± 0.4 Gt/yr^2. For WA, ΔM^* acceleration is -24.0 ± 2.2 Gt/yr^2, and P^* acceleration is -14.4 ± 1.4 Gt/yr^2. Ice discharge acceleration for WA is still large, about -9.6 Gt/yr^2. For WA and AP together, ΔM^* acceleration is -29.9 ± 2.6 Gt/yr^2, while the P^* effect is -15.4 ± 1.4 Gt/yr^2. The conclusion is that both precipitation decrease and ice discharge increase are important to ice mass loss acceleration for both AP and WA. Acceleration rates for the Amundsen Sea (AS) sector and other regions of WA are also given in Table 1, showing that most WA acceleration is associated with this area. The estimated acceleration rates here agree well with those reported by *Schrama et al*. [2014].

EA and WA ΔM^* accelerations are of opposite sign, with an EA value of 16.3 ± 5.7 Gt/yr^2. P^* is 7.2 ± 1.8 Gt/yr^2, accounting for less than half the EA rate. A similar acceleration difference was reported previously [*Velicogna et al*., 2014]. Decreasing ice discharge rates in EA could be a cause, but remote sensing [*Rignot et al*., 2008] and ground-based observations do not indicate this. Another possibility is that atmospheric mass variations have not been completely removed from GRACE, due to errors in the atmospheric pressure fields used in the dealiasing process [*Duan et al*., 2012; *Schrama and Visser*, 2007; *Velicogna et al*., 2001]. This might leave an erroneous atmospheric signal in ΔM^* with a small amplitude but large spatial scale. When integrated over time, low-frequency variations would be amplified in ΔM^* and contaminate acceleration estimates. This possibility is examined in the next section.

3.2. Mass Change Empirical Orthogonal Function Analysis

Here we use scale-factor-adjusted GRACE estimates of $\Delta M^T_{T_0}$ integrated and reduced to ΔM^* to examine time-space patterns of interannual variations in Figure 4. Combined empirical orthogonal functions (CEOFs) [*Kutzbach*, 1967] are obtained from ΔM^* and P^*. Gridded P^* are obtained using a SH degree 60 expansion

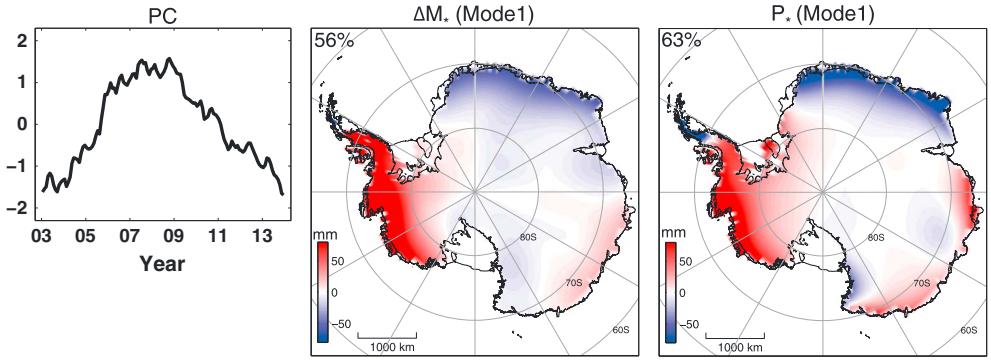

Figure 4. Principal component (PC) and spatial pattern of the first mode from combined EOF (CEOF) with the anomalous ΔM^* and P^*.

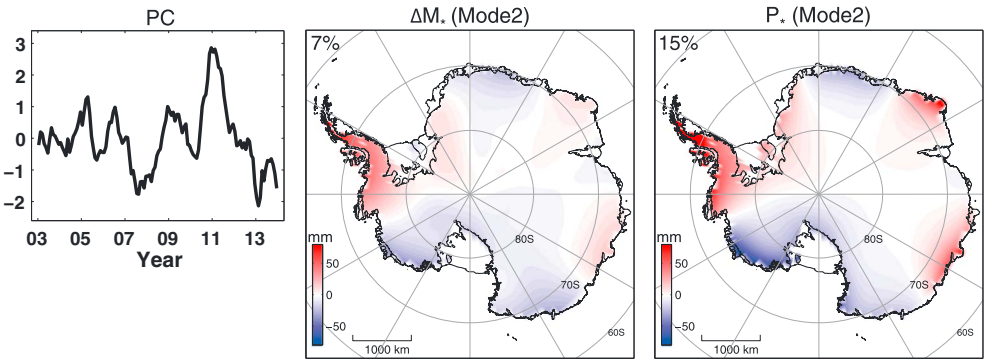

Figure 5. Principal component (PC) and spatial pattern of the second mode from combined EOF (CEOF) with the anomalous ΔM^* and P^*.

of the original data, with 300 km Gaussian smoothing, evaluated at grid points, and multiplied by scale factors. Principal component (PC) time series are scaled to unit variance. CEOF spatial patterns are in units of millimeter of water layer thickness or kg/m^2. In CEOF analysis, modes are found, which share a common PC, but have separate spatial patterns. Figure 4 shows the first PC and CEOF for ΔM^* and P^*. This first mode accounts for 56% of ΔM^* and 63% of P^* variances, and the covariance is 60%. The PC shows a quadratic shape implying acceleration of mass loss. Both CEOF spatial modes show a positive pattern in WA and negative in EA, implying accelerating loss in WA and decelerating in EA. That is, the mode depicts precipitation or mass accumulation *rates* decreasing in WA and increasing in EA. In WA, the largest first-mode amplitudes are near the Bellinghausen Sea (BS) and southern AP. Terre Adelie (TA) and Queen Mary Land show variations of the same sign but with smaller magnitudes. Negative mode values (increasing rates of mass accumulation) are seen around DML [*Boening et al.*, 2012; *Lenaerts et al.*, 2012] over much of EA and small regions in the AP.

Figure 5 shows the second mode. The PC shows interannual variations with periods of 2–3 years. Variance fractions for ΔM^* and P^* are 7% and 15%, respectively, and covariance is 11%. Spatial pattern shows smaller positive and negative anomalous patterns relative to the first mode with negative anomalies in the AS and DML and positive anomalies in the BS, AP, EA, TA, and Wilkes Land. Spatial patterns of ΔM^* and P^* remain similar. Considering the PCs and spatial patterns of both modes, CEOF indicates that interannual and longer-period variations in ice mass change are largely associated with changes in net surface accumulation from 2003 to 2013 as shown in Figure 3.

The residual field, $\Delta M^* - P^*$ ($=-D^*$), should be an estimate of ice mass change associated with ice discharge rate variations. There are clear signals in AP and WA (not shown) in the residual field, but their amplitudes are smaller than the forward modeling estimates. Presumably, the scale factor method is not able to correct leakage effects that are especially important along the coast. The residual field likely includes mass variations other than precipitation. Among these may be residual atmospheric pressure effects [*Schrama and Visser*, 2007; *Velicogna et al.*, 2001]. GRACE observations are measures of vertically integrated mass change including both ice and atmospheric mass. Atmospheric mass effects are intended to be removed during GRACE dealiasing, but the process may be imperfect. Evidence of this is that operational European Centre for Medium-Range Weather Forecasts (ECMWF) pressure fields used in GRACE dealiasing show spurious step changes [*Duan et al.*, 2012] which could introduce apparent accelerations in ΔM^*.

To look for further evidence of residual atmospheric pressure effects in ΔM^*, we apply 600 km Gaussian smoothing to $\Delta M^* - P^*$, which should include both anomalous ice discharge and uncorrected atmospheric mass effects. Empirical orthogonal function (EOF) decomposition is used to distinguish the two components. Analysis of the second and third EOF modes suggests a connection with ice discharge, because amplitudes are largest near the coast. These modes are not shown, and further analysis of them would require correction for spatial leakage. The first EOF mode (variance fraction 42%) shows a pattern (Figure 6, top) with the same sign of over most of Antarctica. This spatial pattern is suggestive of error in atmospheric pressure. The first-mode PC shows oscillations at periods shorter than 1 year, superimposed

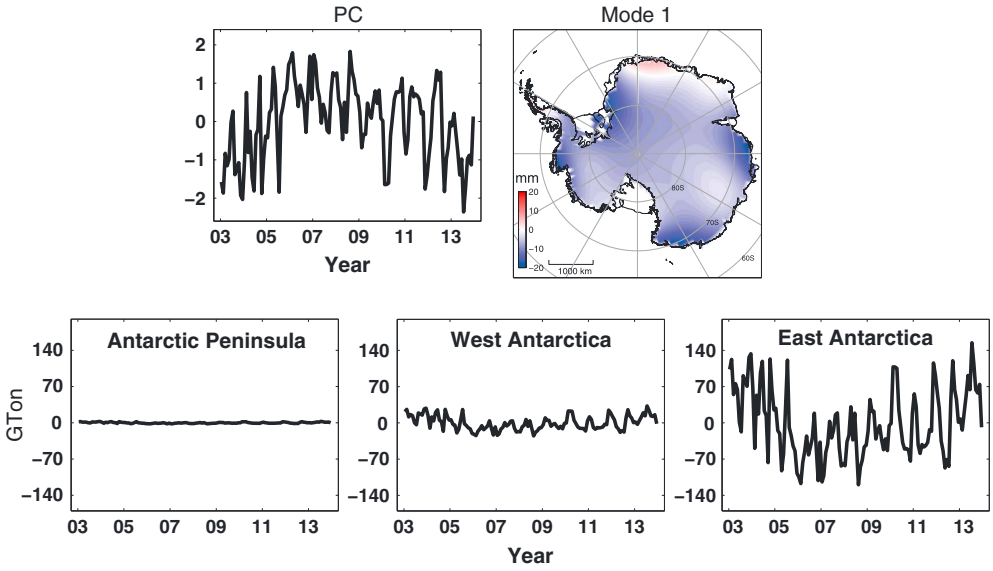

Figure 6. (top) PC and EOF of the first mode of $\Delta M^* - P^*$ after smoothing by a 600 km Gaussian filter. (bottom) Residual ice mass variations recovered from the first EOF mode of $\Delta M^* - P^*$ in AP, WA, and EA.

on a quadratic variation indicating mass acceleration. The bottom plots of the figure show residual ice mass variations in the AP, WA, and EA recovered from the first mode of $\Delta M^* - P^*$. There is no clear variation in the AP and WA, but in EA, evident acceleration patterns are present. The acceleration rates in the AP, WA, and EA are 0.1 ± 0.2 Gt/yr^2, 1.7 ± 1.2 Gt/yr^2, and 8.0 ± 4.7 Gt/yr^2, respectively. In particular, the acceleration rate in EA is about the size of the EA acceleration discrepancy in Table 1.

The first mode shown in Figure 6 is likely associated with error in operational ECMWF surface pressure fields used in GRACE dealiasing processing. *Duan et al.* [2012] noted that ECMWF surface pressure error would be important in the AP and Transantarctic Mountains (TM) regions, but EOF analysis (Figure 6) shows that the contamination is probably continent wide. This suggests that apparent accelerations are not related to known ECMWF errors in the AP and TM. To examine further whether an acceleration error is due to ECMWF model error or some other cause, we compare three barometric surface pressure fields, ERA Interim, MERRA, and NCEP/DOE, which are available for Antarctica. ERA Interim is a reanalysis version of ECMWF fields as used in GRACE dealiasing processing. Therefore, we assume that atmospheric pressure error estimates for ΔM^* are represented by the two differences: MERRA-ERA Interim and NCEP/DOE-ERA Interim. If the PC and EOF modes shown in Figure 6 are associated with ECMWF surface pressure error, the two error estimates ought to show similar spatial patterns and temporal variations. EOF first-mode PCs and spatial patterns for these two are shown in Figure 7. Both PCs have similar temporal variations, with each other, and with the PC in Figure 6. Similarly, spatial patterns resemble those in Figure 6 with a common

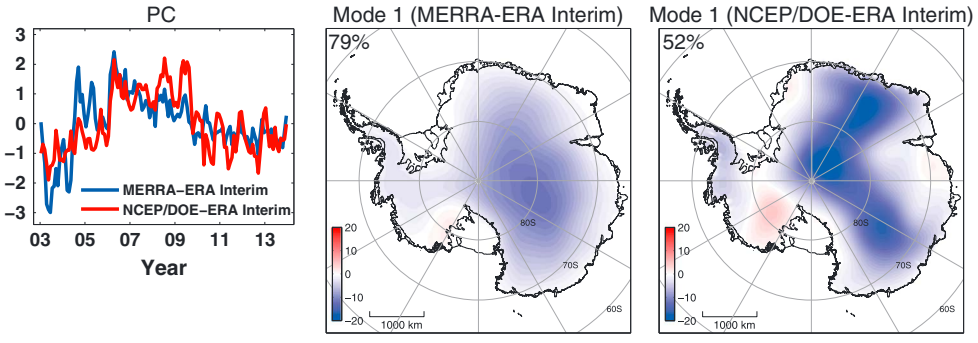

Figure 7. The first PCs and EOF modes of the differences of atmospheric pressure fields, MERRA-ERA Interim and NCEP/DOE-ERA Interim.

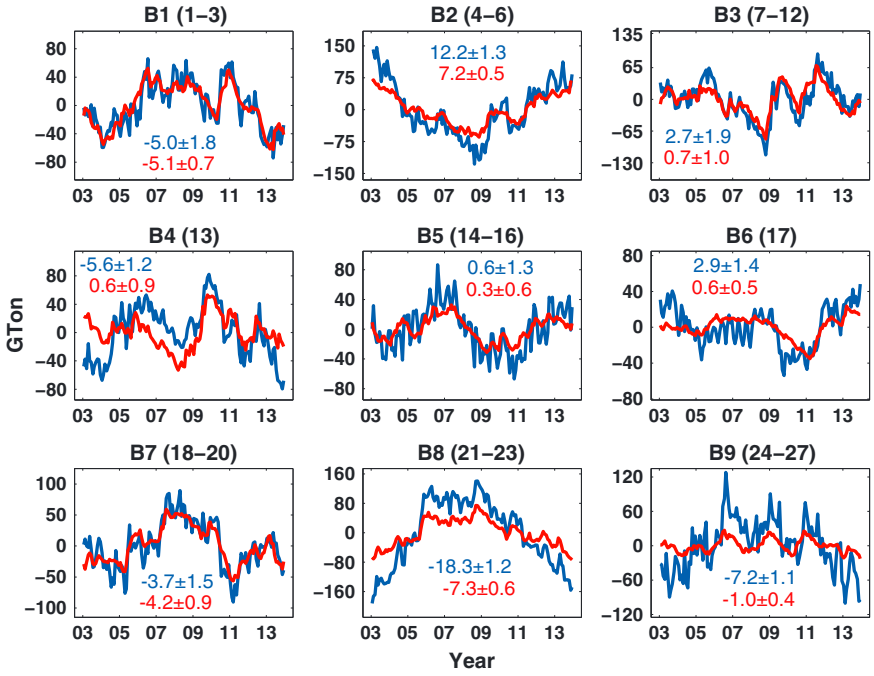

Figure 8. Ice mass variation (ΔM^*) after atmospheric pressure error corrections and precipitation accumulation (P^*) in regions B1–B9.

sign over most of the continent. Acceleration rates in EA from MERRA-ERA Interim and NCEP/DOE-ERA Interim are 6.9 ± 1.5 Gt/yr^2 and 10.8 ± 2.1 Gt/yr^2, respectively, comparable to the Table 1 EA acceleration discrepancy. AP and WA accelerations associated with these pressure field differences are much smaller. Figures 6 and 7 together indicate that Antarctic barometric pressure signals remain in GRACE estimates and are the likely source of EA acceleration discrepancies.

We can use the first EOF mode of $\Delta M^* - P^*$ (shown in Figure 6) as an estimate of residual barometric pressure in GRACE estimates and use this to modify ΔM^* in the nine regions, B1–B9. These are compared with P^* in Figure 8. Now in most regions, the time series of ΔM^* show more similar variations to P^* when compared with Figure 3. Note that high-frequency variations are also suppressed, particularly in region B1 (Basins 1–3). The combined regional acceleration rates for the AP, WA, and EA can similarly be adjusted as shown in Table 1 (in italics). After this atmospheric pressure error correction, the total Antarctic acceleration rate increases significantly, from −13.6 ± 7.2 Gt/yr^2 to −23.3 ± 6.3 Gt/yr^2. This is mostly due to the decrease of a positive acceleration rate in EA from 16.3 ± 5.7 Gt/yr^2 to 8.4 ± 5.0 Gt/yr^2.

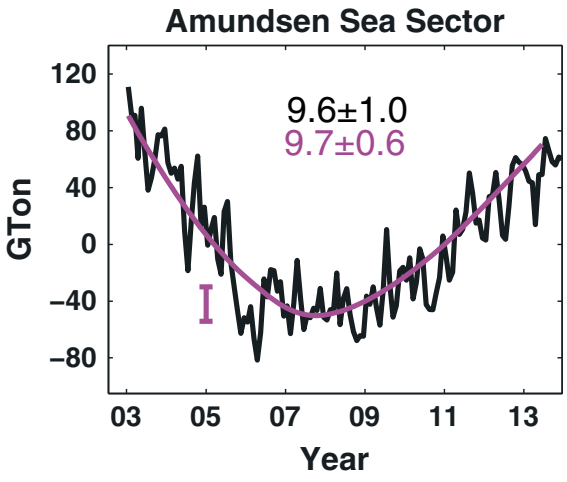

Figure 9. The black lines show variations of accumulated ice discharge in the Amundsen Sea sector (Basins 21 and 22) after removing linear trends and seasonal cycles. The magenta lines show similar ice discharge variations estimated by ice flow velocity and thickness for two of these [*Mouginot et al.*, 2014].

Some low-frequency variations in ΔM^* (after atmospheric pressure error correction) not accounted for by P^* may be due to variations in ice discharge rates, likely for basins near the AS [*Mouginot et al.*, 2014]. We can calculate an anomalous ice discharge accumulation ($D^* = P^* - \Delta M^*$) for the AS (Basins 21 and 22).

The black line in Figure 9 shows time the series of D^* estimated in this way. It exhibits a parabolic shape indicating acceleration of ice discharge from 2003 to 2013. Values of D^* can be compared with *Mouginot et al*. [2014], in which estimated annual discharge in Basins 21 and 22 was derived from velocity and thickness at grounding lines. To compare with our D^*, we first integrate annual discharges [*Mouginot et al*., 2014] and remove linear trends. Residual discharge in Figure 9 (magenta lines) is very similar to D^*, showing AS accelerations of similar magnitudes. Discharge acceleration rates estimated in this study and *Mouginot et al*. [2014] are 9.6 ± 1.0 Gt/yr^2 and 9.7 ± 0.6 Gt/yr^2, respectively. Therefore, the difference between ΔM^* and P^* is likely associated with ice discharge in this area. The continent total Antarctic acceleration rate in ice discharge is about -15.1 ± 6.5 Gt/yr^2, larger than the previous estimate, -9.0 ± 1.0 Gt/yr^2 during 1992–2009 [*Rignot et al*., 2011]. Regional ice discharge accelerations are also summarized in Table 1.

4. Conclusions

The focus of this study is to understand the apparent AIS mass loss acceleration over the last decade that is evident in GRACE observations. Integration over time of NCEP/DOE, ERA Interim, and MERRA precipitation fields provides estimates of precipitation accumulation in the GRACE era. Removing linear trends and seasonal cycles leaves residual variations whose quadratic components represent apparent acceleration. For much of the AIS, mass change acceleration appears related to precipitation anomalies. The exceptions are the AP and WA, where ice discharge acceleration is important. In WA, loss acceleration (-25.7 ± 2.3 Gt/yr^2) is due to both precipitation decrease (-14.4 ± 1.4 Gt/yr^2) and ice discharge rate increase (-11.3 ± 2.7 Gt/yr^2). In the AP, ice discharge rate acceleration appears to dominate.

Over most of EA, apparent GRACE acceleration of ice mass rates is explained by precipitation increases and incomplete removal of barometric pressure signals in GRACE processing. Without correcting for estimated barometric pressure residuals in GRACE, the mass acceleration rate for the entire AIS from 2003 to 2013 would be about -13.6 ± 7.2 Gt/yr^2. Using our estimate of residual barometric pressure error, AIS-estimated acceleration is larger, -23.3 ± 6.3 Gt/yr^2. This is a combination of ice discharge rate increase (-15.1 ± 6.5 Gt/yr^2) and precipitation decrease (-8.2 ± 2.0 Gt/yr^2).

Wouters et al. [2013] suggested that the period of satellite observations is too short to project future sea level rise due to the stochastic nature of ice sheet weather. We have shown that the GRACE AIS acceleration rate is influenced by both precipitation accumulation and uncorrected atmospheric pressure residuals. The sign of SMB "weather" (precipitation) and barometric pressure errors may vary over time scales comparable to the era of satellite observations, while the sign of ice discharge acceleration, related to ice dynamics, would be expected to persist over decadal time scales. In this case, the present acceleration rate related to ice dynamics would lead to about 8 ± 3.0 cm of global sea level increase by 2050. This is a larger contribution than the increase arising from continued loss at the linear rate estimated in the GRACE era (about 4 cm sea level rise by 2050 using -162.8 ± 30.0 Gt/yr with ICE-5G GIA corrections).

Acknowledgments
This work was supported by National Research Foundation grant NRF-2013R1A1A2008368 and Korea Polar Research Institute research grant PM14020. D.W. and B.T.'s contributions were carried out on behalf of the Jet Propulsion Laboratory, California Institute of Technology, under a contract with NASA. GRACE, ERA Interim, MERRA, and NCEP/DOE data are available from GRACE Tellus site (http://grace.jpl.nasa.gov), ECMWF data server (http://data-portal.ecmwf.int), Goddard Earth Sciences Data and Information Services Center (http://disc.sci.gsfc.nasa.gov), and Earth System Research Laboratory (http://www.esrl.noaa.gov), respectively. RACMO2.3 data are available upon request in Institute for Marine and Atmospheric Research Utrecht (http://www.projects.science.uu.nl/iceclimate/models/antarctica.php).

References

A, G., J. Wahr, and S. Zhong (2013), Computations of the viscoelastic response of a 3-D compressible Earth to surface loading: An application to glacial isostatic adjustment in Antarctica and Canada, *Geophys. J. Int.*, *1–16*, doi:10.1093/gji/ggs030.

Bamber, J., and W. P. Aspinall (2013), An expert judgment assessment of future sea level rise from the ice sheets, *Nat. Clim. Change*, *3*, 424–427.

Boening, C., M. Lebsock, F. Landerer, and G. Stephens (2012), Snowfall-driven mass change on the East Antarctic Ice Sheet, *Geophys. Res. Lett.*, *39*, L21501, doi:10.1029/2012GL053316.

Chen, J. L., C. R. Wilson, and B. D. Tapley (2013), Contribution of ice sheet and mountain glacier melt to recent sea level rise, *Nat. Geosci.*, *6*, 549–552, doi:10.1038/NGEO1829.

Cheng, M., and B. D. Tapley (2004), Variations in the Earth's oblateness during the past 28 years, *J. Geophys. Res.*, *109*, B09402, doi:10.1029/2004JB003028.

Duan, J., C. K. Shum, J. Guo, and Z. Huang (2012), Uncovered spurious jumps in the GRACE atmospheric de-aliasing data: Potential contamination of GRACE observed mass change, *Geophys. J. Int.*, *191*, 83–87, doi:10.1111/j.1365-246X.2012.05640.x.

Fettweis, X., E. Hanna, E. Lang, A. Belleflamme, M. Erpicum, and H. Gallée (2013), Important role of the mid-tropospheric circulation in the recent surface melt increase over the Greenland Ice Sheet, *Cryosphere*, *7*, 241–248, doi:10.5194/tc-7-241-2013.

Kanamitsu, M., W. Ebisuzaki, J. Woollen, S.-K. Yang, J. J. Hnilo, M. Fiorino, and G. L. Potter (2002), NCEP-DOE AMIP-II reanalysis (R-2), *Bull. Am. Meteorol. Soc.*, 1631–1643.

King, M., R. Bingham, P. Moore, P. Whitehouse, M. Bentley, and G. Milne (2012), Lower satellite-gravimetry estimates of Antarctic sea-level contribution, *Nature*, *491*(7425), 586–589, doi:10.1038/nature11621.

Kutzbach, J. E. (1967), Empirical eigenvectors of sea-level pressure, surface temperature and precipitation complexes over North America, *J. Appl. Meteorol.*, *6*(5), 791–802.
Lee, H., C. K. Shum, I. Howat, A. Monaghan, Y. Ahn, J. Duan, J.-Y. Guo, C.-Y. Kuo, and L. Wang (2012), Continuously accelerating ice loss over Amundsen Sea catchment, West Antarctica, revealed by integrating altimetry and GRACE data, *Earth Planet. Sci. Lett.*, *321–322*, 74–80.
Lenaerts, J. T. M., M. R. van den Broeke, W. J. van de Berg, E. van Meijgaard, and P. K. Munneke (2012), A new, high-resolution surface mass balance map of Antarctica (1979–2010) based on regional atmospheric climate modeling, *Geophys. Res. Lett.*, *39*, L04501, doi:10.1029/2011GL050713.
Medley, B., et al. (2013), Airborne-radar and ice-core observations of annual snow accumulation over Thwaites Glacier, West Antarctica confirm the spatiotemporal variability of global and regional atmospheric models, *Geophys. Res. Lett.*, *40*, 3649–3654, doi:10.1002/grl.50706.
Mouginot, J., E. Rignot, and B. Scheuchl (2014), Sustained increase in ice discharge from the Amundsen Sea Embayment, West Antarctica, from 1973 to 2013, *Geophys. Res. Lett.*, *41*, 1576–1584, doi:10.1002/2013GL059069.
Palerme, C., J. E. Kay, C. Genthon, T. L'Ecuyer, N. B. Wood, and C. Claud (2014), How much snow falls on the Antarctic Ice Sheet?, *Cryosphere*, *8*, 1577–1587, doi:10.5194/tc-8-1577-2014.
Pritchard, H. D., R. J. Arthern, D. G. Vaughan, and L. A. Edwards (2009), Extensive dynamic thinning on the margins of the Greenland and Antarctic Ice Sheets, *Nature*, *461*, 971–975.
Pritchard, H. D., S. R. M. Ligtenberg, H. A. Fricker, D. G. Vaughan, M. van den Broeke, and L. Padman (2012), Antarctic ice-sheet loss driven by basal melting of ice shelves, *Nature*, *484*, 502–505, doi:10.1038/nature10968.
Rienecker, M. M., et al. (2011), MERRA: NASA's Modern-Era Retrospective Analysis for Research and Applications, *J. Clim.*, *24*, 3624–3648, doi:10.1175/JCLI-D-11-00015.1.
Rignot, E., J. Bamber, M. van den Broeke, C. Davis, Y. Li, W. J. van de Berg, and E. van Meijgaard (2008), Recent Antarctic ice mass loss from radar interferometry and regional climate modelling, *Nat. Geosci.*, *1*, 106–110.
Rignot, E., I. Velicogna, M. van den Broeke, A. Monaghan, and J. T. M. Lenaerts (2011), Acceleration of the contribution of the Greenland and Antarctic Ice Sheets to sea level rise, *Geophys. Res. Lett.*, *38*, L05503, doi:10.1029/2011GL046583.
Sasgen, I., H. Dobslaw, Z. Martinec, and M. Thomas (2010), Satellite gravimetry observation of Antarctic snow accumulation related to ENSO, *Earth Planet. Sci. Lett.*, *299*, 352–358.
Sasgen, I., M. van den Broeke, J. L. Bamber, E. Rignot, L. S. Sorensen, B. Wouters, Z. Martinec, I. Velicogna, and S. B. Simonsen (2012), Timing and origin of recent regional ice-mass loss in Greenland, *Earth Planet. Sci. Lett.*, *333–334*, 293–303, doi:10.1016/j.epsl.2012.03.033.
Schrama, E. J. O., and P. Visser (2007), Accuracy assessment of the monthly GRACE geoids based upon a simulation, *J. Geod.*, *81*, 67–80.
Schrama, E. J. O., B. Wouters, and R. Rietbroek (2014), A mascon approach to assess ice sheet and glacier mass balances and their uncertainties from GRACE data, *J. Geophys. Res. Solid Earth*, *119*, 6048–6066, doi:10.1002/2013JB010923.
Shepherd, A., et al. (2012), A reconciled estimate of ice-sheet mass balance, *Science*, *338*(30), 1183–1189.
Simmons, A., S. Uppala, D. Dee, and S. Kobayashi (2007), ERA-Interim: New ECMWF reanalysis products from 1989 onwards ECMWF Newsletter No. 110.
Swenson, S., and J. Wahr (2006), Post-processing removal of correlated errors in GRACE data, *Geophys. Res. Lett.*, *33*, L08402, doi:10.1029/2005GL025285.
Swenson, S., D. Chambers, and J. Wahr (2008), Estimating geocenter variations from a combination of GRACE and ocean model output, *J. Geophys. Res.*, *113*, B08410, doi:10.1029/2007JB005338.
Velicogna, I. (2009), Increasing rates of ice mass loss from the Greenland and Antarctica Ice Sheets revealed by GRACE, *Geophys. Res. Lett.*, *36*, L19503, doi:10.1029/2009GL040222.
Velicogna, I., and J. Wahr (2013), Time-variable gravity observations of ice sheet mass balance: Precision and limitations of the GRACE satellite data, *Geophys. Res. Lett.*, *40*, 3055–3063, doi:10.1002/grl.50527.
Velicogna, I., J. Wahr, and H. Van den Dool (2001), Can surface pressure be used to remove atmospheric contributions from GRACE data with sufficient accuracy to recover hydrological signals?, *J. Geophys. Res.*, *106*(B8), 16,415–416,434, doi:10.1029/2001JB000228.
Velicogna, I., T. C. Sutterley, and M. R. van den Broeke (2014), Regional acceleration in ice mass loss from Greenland and Antarctica using GRACE time-variable gravity data, *Geophys. Res. Lett.*, *41*, 8130–8137, doi:10.1002/2014GL061052.
van Wessem, J. M., et al. (2014), Improved representation of East Antarctic surface mass balance in a regional atmospheric climate model, *J. Glaciol.*, *60*(222), 761–770, doi:10.3189/2014JoG14J051.
Williams, S., P. Moore, M. King, and P. Whitehouse (2014), Revisiting GRACE Antarctic ice mass trends and accelerations considering autocorrelation, *Earth Planet. Sci. Lett.*, *385*, 12–21, doi:10.1016/j.epsl.2013.10.016.
Wouters, B., J. L. Bamber, M. R. van den Broeke, J. T. M. Lenaerts, and I. Sasgen (2013), Limits in detecting acceleration of ice sheet mass loss due to climate variability, *Nat. Geosci.*, *6*, 613–616, doi:10.1038/NGEO1874.
Zwally, H. J., M. B. Giovinetto, M. A. Beckley, and J. Saba (2012), Antarctic and Greenland drainage systems GSFC Cryospheric Sciences Laboratory. [Available at http://icesat4.gsfc.nasa.gov/cryo_data/ant_grn_drainage_systems.php.]